Microglial phospholipase D4 deficiency influences myelination during brain development

By Terumasa Chiba,[*1,‡] Yoshinori Otani,[*1,‡] Yoshihide Yamaguchi,[*1] Tomoko Ishibashi,[*1] Akiko Hayashi,[*1] Kenji F. Tanaka,[*2] Maya Yamazaki,[*3] Kenji Sakimura[*3] and Hiroko Baba[*1,†]

(Communicated by Kunihiko Suzuki, m.j.a.)

Abstract: Phospholipase D4 (PLD4) is expressed in activated microglia that transiently appear in white matter during postnatal brain development. Previous knockdown experiments using cultured microglia showed PLD4 involvement in phagocytosis and proliferation. To elucidate the role of PLD4 *in vivo*, PLD4-deficient mice were generated and the cerebella were examined at postnatal day 5 (P5) and P7, when PLD4 expression is highest in microglia. Wild type microglia showed strong immunoreactivity for microglial marker CD68 at P5, whereas CD68 signals were weak in PLD4-deficient microglia, suggesting that loss of PLD4 affects microglial activation. At P5 and P7, immunostaining for anti-myelin basic protein (MBP) antibody indicated a mild but significant delay in myelination in PLD4-deficient cerebellum. Similar change was also observed in the corpus callosum at P7. However, this difference was not apparent at P10, suggesting that microglial PLD4-deficiency primarily influences the early myelination stage. Thus, microglia may have a transient role in myelination via a PLD4-related mechanism during development.

Keywords: phospholipase D, microglia, myelin, brain, development

Introduction

Phospholipase D4 (PLD4) is a recently identified PLD family member that was originally found by searching the cerebellar development transcriptome database (CDT-DB) for characteristic spatiotemporal gene expression patterns during mouse cerebellar development.[1),2)] PLD4 is classified within the PLD family because it contains two conserved His-X-Lys-$(X)_4$-Asp (HKD) motifs that are critical for PLD enzyme activity.[2)] However, PLD4 does not display

*1   Department of Molecular Neurobiology, Tokyo University of Pharmacy and Life Sciences, Tokyo, Japan.

*2   Department of Neuropsychiatry, School of Medicine, Keio University, Tokyo, Japan.

*3   Department of Cellular Neurobiology, Brain Research Institute, Niigata University, Niigata, Japan.

†   Correspondence should be addressed to: H. Baba, Department of Molecular Neurobiology, Tokyo University of Pharmacy and Life Sciences, 1432-1 Horinouchi, Hachioji, Tokyo 192-0392, Japan (e-mail: hirobaba@toyaku.ac.jp).

‡   These two authors equally contributed to this work.

Abbreviations: PLD4: phospholipase D4; Iba1: ionized calcium binding adaptor molecule 1; MBP: myelin basic protein; CD68: cluster of differentiation 68; BAC: bacterial artificial chromosome; tetO: tetracycline operator; GFAP: glial fibrillary acidic protein; HE: hematoxylin/eosin.

PLD activity that catalyzes the conversion of phosphatidylcholine into choline and phosphatidic acid. The protein structure of PLD4 is also different from PLD1 and PLD2, since PLD4 is a glycoprotein with a single transmembrane domain and does not contain Phox homology (PX) or pleckstrin homology (PH) domains, both of which are involved in membrane targeting and activation of PLD.[3)] In addition to its expression in developing brain, PLD4 mRNA is expressed in mouse spleen, liver, lung, and thymus at postnatal day 7 (P7). Recently, it was reported that the *PLD4* gene is an indicator of susceptibility to certain autoimmune diseases in a Japanese population,[4)] and a nonsense mutation in *PLD4* gene was shown to cause a zinc deficiency-like syndrome in cattle.[5)] However, the roles of PLD4 in these disorders as well as in normal brain development are still unknown.

The expression pattern of PLD4 is tightly regulated during brain development. In mouse cerebellum, PLD4 mRNA expression gradually increases after birth, peaks at P7, and is significantly reduced thereafter.[2),6)] At P7, expression is restricted to microglia in the white matter. In an *in vitro* culture system, PLD4 expression increased in acti-

vated microglia.[6] This protein was upregulated in nuclei and cytoplasmic vesicles with early endosomal markers after lipopolysaccharide stimulation. When bioparticles were added, PLD4 accumulated in phagosomes during phagocytosis. Inhibition of PLD4 expression by specific siRNA treatment affected proliferation and phagocytosis of microglia by lipopolysaccharide stimulation.[6] However, the functional relevance of PLD4 upregulation during development is undetermined. It is well known that transient microglial activation occurs in the normal developing rodent brain,[7]–[10] as like indicated by the expression of PLD4 mRNA.[6] These activated microglia are believed to play a role in the clearance of apoptotic cells, neurite growth, and synaptic or axonal pruning.[11]–[16] At P7 in the mouse cerebellum, where PLD4-positive activated microglia are present, myelination is ongoing and apoptosis of excess oligodendrocytes occurs in addition to axonal pruning. Myelination process is regulated by local environment.[17]–[19] Therefore, the presence of activated microglia at this stage of development suggests their involvement in myelination.

In the present study, we generated PLD4-deficient mice to understand the role of this protein in activated microglia during brain development. The influences of PLD4-deficient microglia on various cell types and myelination were examined in the developing cerebellum and corpus callosum.

Materials and methods

Preparation of the PLD4-targeting vector for generating PLD4 knock-in mice. For preparation of the PLD4-targeting vector, a bacterial artificial chromosome (BAC) vector containing the mouse *PLD4* gene was purchased from the Children's Hospital Oakland Research Institute (Oakland, CA). A PLD4 target vector including the diphtheria toxin A subunit (DTA) was constructed using the Flexible Accelerated STOP Tetracycline Operator (tetO)-knockin (FAST) system.[20] Briefly, a loxP-FRT-Neo-STOP-FRT-tetO-loxP cassette (3.5 kb, Fig. 1A) was inserted immediately upstream of the translation initiation site of the *PLD4* gene in a BAC vector by conventional homologous recombination using two plasmids containing STOP-tetO cassette (pNeoSTOPtetO) and pBADTc TypeG. The *PLD4* gene including regions 6 kb upstream and 4 kb downstream of the translation initiation site was then extracted using a retrieve vector, pMCS-DTA plasmid and constructed PLD4-targeting vector.

Homologous recombination in embryonic stem (ES) cells. PLD4 knock-in mice were generated by the method described previously.[21],[22] The PLD4-targeting vector (0.05 pmol) was transfected into an ES cell line (1×10^5, RENKA) derived from ES cells of C57BL/6N mice[21] by electroporation (Bio-RAD, Hercules, CA) (Supplemental Fig. 1A). Homologous recombinant cells were selected by G418 (175 µg/ml; Sigma-Aldrich Japan, Tokyo, Japan). Ten selected ES cells were individually isolated from each well of a 24-well plate, and the cell lines were prepared. Cells were confluent after 18 days, at which point half of the cells in each well were frozen, and the remaining cells were incubated in lysis buffer [50 mM Tris-HCl, pH 8.0, 100 mM NaCl, 20 mM ethylenediaminetetraacetic acid (EDTA), 1% sodium dodecyl sulfate (SDS)] containing proteinase K (150 µg/mL) at 50 °C overnight. RNase A (10 µg/well) was added to the lysed cells and genomic DNA was isolated from each cell line using the PI-1200 DNA isolator (Kurabo, Osaka, Japan) for Southern blot analysis. Recombinant ES cell clones were identified by Southern blot analysis using a 5′-probe on EcoRV-digested genomic DNA for the first screening, and a 3′-probe on KpnI, EcoRI, or SpeI-digested genomic DNA and a 5′-probe on BstEII-digested genomic DNA for the second screening (sequence of each probe is available in Supporting information). Chimeric mice were generated using methods described previously.[22] Genotypes were verified by Southern blotting using a 5′-probe on EcoRV-digested genomic DNA and a 3′-probe on KpnI-digested genomic DNA (Supplemental Fig. 1).

Animals. PLD4-deficient mice were maintained on a C57BL/6N background. Genotypes were determined by PCR of mouse tail genomic DNA using KOD FX Neo (Toyobo Life Science; Osaka Japan) with the following primer sets:
PLD4 upstream primer: 5′-TGGAAGCCATTC-TAGGGCTGTGAA-3′
tetO upstream primer: 5′-AGCAGAGCTCGTT-TAGTGAACCGT-3′
PLD4 downstream primer: 5′-AAGTGACCGAG-GCAGCTTCAGAAA-3′.

The primer set of PLD4-upstream and -downstream primers generates 1.5-kbp PCR product from wild type genomic DNA. The primer set of tetO-upstream and PLD4-downstream primers generates 850-bp PCR product from recombinant genomic DNA. Both PCR fragments are produced in heterozygote sample.
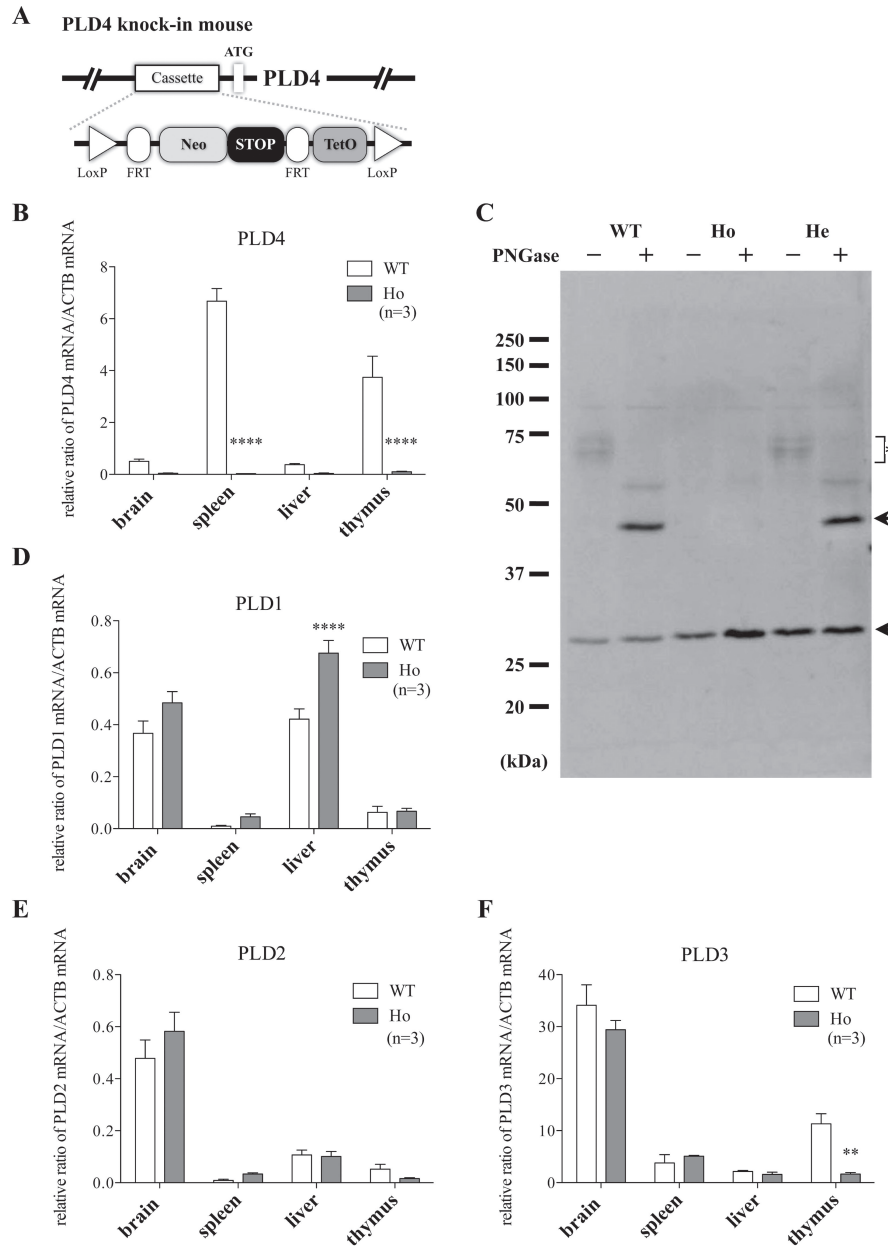
Fig. 1.   Generation of PLD4-deficient mice. **(A)** Genome structure of the *PLD4* gene generated by homologous recombination of the STOP-tetO cassette in PLD4 knock-in (PLD4-deficient) mice. **(B)** Expression of PLD4 mRNA by quantitative real time PCR (qRT-PCR) in brain, spleen, liver and thymus of adult wild type (WT) and PLD4-deficient (Ho) mice. Graphs show the relative ratio of the level of PLD4 and β-actin mRNA from samples run in triplicate from 3 independent experiments. In wild type, PLD4 mRNA was expressed in brain and various reticuloendothelial tissues, including the spleen, liver and thymus. In PLD4-deficient mice, PLD4 mRNA was completely eliminated in these tissues. **(C)** PLD4 protein levels in adult wild type (WT), homozygote (Ho), and heterozygote (He) mice. Spleen homogenates (10 µg) with or without deglycosylation were separated by 10.5% sodium dodecylsulfate polyacrylamide gel electrophoresis (SDS-PAGE) and Western blot analysis was performed using an anti-PLD4 antibody. Since PLD4 has multiple glycosylation sites, various PLD4-related bands (70–75 kDa; indicated by *) were shown in non-treated samples. The arrow indicates deglycosylated PLD4 ($\sim$45 kDa) by PNGase F (peptide-N-glycosidase F) treatment. The arrowhead indicates an unrelated protein product detected by the anti-PLD4 antibody. Note that this protein was also detected in PLD4-deficient spleen samples while PLD4 bands with or without sugars were completely eliminated. **(D–F)** Expression patterns of PLD1 (D), PLD2 (E), and PLD3 (F) mRNA in adult mice were examined by qRT-PCR. The quantitative analyses shown in B to F were obtained from three independent experiments. All experiments were performed in triplicate. Graphs indicate the mean ± standard error of the mean (SEM). Two-way ANOVA with Bonferroni multiple comparison tests were used for statistical analyses. ****P < 0.0001, **P < 0.01.

Homozygous and wild type mice were used in this study and heterozygous animals were used for maintenance of the colony. Littermates or age-matched wild type mice were used as control animals. The mouse line was maintained in a designated specific pathogen–free environment at the animal facility of the Tokyo University of Pharmacy and Life Sciences under the university guidelines for care and use of animals. All animal protocols were approved by the Institutional Animal Use Committee at Tokyo University of Pharmacy and Life Sciences (approval number: P12-23, P13-31, P14-09, P15-26).

Antibodies. The following antibodies were used for immunohistological studies: rabbit polyclonal anti-ionized calcium binding adaptor molecule 1 (Iba1) antibody (1:800; Wako, Osaka, Japan); rat monoclonal anti-myelin basic protein (MBP) antibody (1:100; Chemicon/Merck Millipore, Darmstadt, Germany); rabbit polyclonal anti-PLD4 C-terminal antibody (1:200) which was produced by immunization with 16 amino acid residues (from amino acid 488 to 503, YAMDLDRQVPSQDCVW) of PLD4;[2] rat monoclonal anti-cluster of differentiation 68 (CD68) antibody (1:100; Abcam, Cambridge, UK); rabbit polyclonal anti-calbindin D-28K antibody (1:200; Chemicon); rabbit polyclonal anti-glial fibrillary acidic protein (GFAP) antibody (1:10; Chemicon); goat polyclonal anti-arginase 1 antibody (1:50; Santa Cruz Biotechnology); biotinylated species-specific secondary antibodies (1:250; Vector Laboratories, Burlingame, CA); Alexa 488- and 594-conjugated species-specific secondary antibodies (1:2000; Molecular Probes/Thermo Fisher Scientific, Waltham, MA). For Western blotting: rat monoclonal anti-MBP antibody (1:4000; Chemicon); rabbit polyclonal anti-β-actin antibody (1:2000; Wako); horseradish peroxidase-conjugated species-specific secondary antibodies (1:10,000; Jackson Immunoresearch, West Grove, PA).

Preparation of mouse brain and spleen homogenates and deglycosylation. Homogenates were prepared from 7-day-old mouse cerebellum and adult mouse spleen. Spleen sample was used to confirm suppression of PLD4 production in the PLD4 knock-in mice because of its abundance in normal condition. All procedures were carried out on ice or at 4 °C. Homogenates were obtained as previously described.[23] Briefly, tissues were homogenized in 9 volumes (wt/vol) of homogenization buffer [0.32 M sucrose, 5 mM Tris-HCl, pH 7.5, 2 mM ethylene glycol-bis(2-aminoethylether)-N,N,N′,N′

tetraacetic acid (EGTA), 0.75 µM aprotinin, 1 µM leupeptin, 1 µM pepstatin, and 0.4 mM phenylmethylsulfonyl fluoride]. The homogenates were centrifuged at 1,000g for 10 min (MX-200; TOMY, Tokyo, Japan) to remove nuclei, and the supernatant was used as the homogenate. All prepared homogenates were stored at -80 °C. Protein concentrations were determined using a bicinchoninic acid (BCA) assay (Pierce Biotechnology/Thermo Fisher Scientific).

Peptide: N-glycosidase F (PNGase F, EC 3.5.1.52) digestion of the peptide was performed as described.[24] The deglycosylated samples were analyzed by Western blotting.

Western blot analysis. Western blotting was performed as previously described[23] with minor modifications. Briefly, each sample was separated on 10.5% or 12% SDS-polyacrylamide gel electrophoresis (SDS-PAGE) and transferred to a polyvinylidene fluoride (PVDF) membrane [Millipore or GE Healthcare UK (Buckinghamshire, UK)]. The membranes were incubated for 1 hr with blocking buffer containing 5% or 0.3% skim milk in 20 mM Tris-HCl (pH 7.4), 150 mM NaCl, and 0.1% Tween 20 (T-TBS) at room temperature. The membranes were then incubated for 1 hr with primary antibodies diluted in blocking buffer and washed three times in T-TBS prior to incubation for 1 hr with secondary antibody in T-TBS. After washing three times in T-TBS, immunoreactivity was detected using the ECL system (GE Healthcare UK). For quantification, band intensities were measured using ImageGauge v4.23 (Fujifilm, Tokyo, Japan).

Immunohistochemistry. Mice were fixed by transcardial perfusion with 4% paraformaldehyde in 0.1 M phosphate buffer, pH 7.4, and brains were post-fixed with the same fixative for 24 hrs. For frozen sections, brains were cryoprotected sequentially in 10% and 20% sucrose in phosphate-buffered saline (PBS), pH 7.4 and embedded in Tissue-Tek OCT compound 4583 (Sakura Finetek, Tokyo, Japan). Tissues were cut into 10-µm-thick frozen sections. Immunofluorescent staining was performed as previously described.[25] Briefly, sections were permeabilized and blocked for 1 hr in PBS containing 0.3% Triton X-100 and 10% normal goat serum. The sections were then incubated overnight at 4 °C with primary antibodies diluted in the blocking solution, thoroughly rinsed in PBS, then incubated with PBS containing fluorescently labeled secondary antibodies and 4′,6-diamidino-2-phenylindole (DAPI; 1:20000) for 1 h at room temperature. Finally, the stained

frozen sections were rinsed and mounted in Vectashield (Vector Laboratories, Burlingame, CA). Images were captured with a confocal FV1000D IX81 laser scanning microscope (Olympus, Tokyo, Japan) or fluorescent microscope (Axio Imager M1 with AxioCam HRc; Carl Zeiss, Oberkochen, Germany).

Paraffin sections (6 µm) were immunostained using methods described previously.[6] Briefly, the sections were incubated for 1 hr in 0.01 M PBS that contained 0.3% Triton X-100 and 10% goat serum (PBS-TGS), then overnight at 4 °C with primary antibodies diluted in PBS-TGS. After rinsing, the sections were incubated with biotinylated secondary antibodies for 30 min at room temperature. They were then incubated with ABC reagent (1:50; Vector Laboratories) for 30 min at room temperature, and immunoreactions were visualized using 0.005% H_2O_2 in 3′3-diaminobenzidine/50 mM Tris buffer for 10 min at RT. Prepared paraffin sections were stained with hematoxylin/eosin (HE). Images were captured using a light microscope (Axio Imager M1 with AxioCam HRc; Carl Zeiss).

For quantification, cells within the white matter of cerebellum or corpus callosum were counted, excluding cerebellar nuclei in the cerebellum. The areas and fluorescent intensities were measured using Image J 1.45. Intensities of all Iba1- or CD68-positive cells in each section were measured as follows: the intensity within each positive cell was measured across the cell at its long axis and the maximum level of intensity in the trace was determined as the intensity of the cell. Intensity is indicated as arbitrary unit (AU).

Quantitative real-time PCR (qRT-PCR). Total RNA was extracted from adult mouse brain, spleen, liver, and thymus using the TRIzol Plus RNA Purification Kit (Invitrogen/Thermo Fisher Scientific). Isolated total RNA was then reverse transcribed with ReverTra Ace reverse transcriptase (Toyobo, Osaka, Japan). RT-PCR was performed with an ABI Prism 7000 (Applied Biosystems, Foster City, CA) using Thunderbird SYBR qPCR mix (Toyobo). Relative expression levels were determined using the comparative cycle threshold (Ct) method according to manufacturer's instructions. β-actin (ACTB) was used as an internal control. The sequences of the RT-PCR primer sets were as follows:

PLD1Real Time F: 5′-ATCGCCAGCTGCACC-GTCAGG-3′
PLD1 Real Time R: 5′-CCACTCCGGTCTGCA-

CGCTG-3′
PLD2Real Time F: 5′-GGGACCTTGCCCGGC-ACTTC-3′
PLD2 Real Time R: 5′-ACACTGCCCGCCTGG-GATCA-3′
PLD3 Real Time F: 5′-ACCAAATCAGCGCCC-AGCCC-3′
PLD3Real Time R: 5′-GAGGGGTTGCTCGTG-GTGGC-3′
PLD4 Real Time F: 5′-TGCCCAGATACGACA-AGTGCCCATG-3′
PLD4 Real Time R: 5′-GTGTCGCCCATCCA-CAACCCAGAA-3′
mACTB Real time F: 5′-GGCTGTATTCCCCT-CCATCG-3′
mACTB Real time R: 5′-CCAGTTGGTAACAA-TGCCATGT-3′

Statistical analysis. Statistical analysis was performed using Excel 2010 (Microsoft) or PRISM 5 (GraphPad). Data were expressed as the mean ± standard error of the mean (SEM). A student t-test or two-way ANOVA followed by Bonferroni multiple comparison tests were performed for comparisons. A p-value of less than 0.05 was regarded as statistically significant.

Results

Generation of PLD4-deficient mice. The PLD4-targeting vector containing a STOP-tetO cassette (Fig. 1A) was used for generation of the PLD4 knock-in mice.[20] For homologous recombination, the PLD4-targeting vector included sequences 6 kb upstream and 4 kb downstream of the *PLD4* gene from the start codon. In front of the start codon located in exon 1, the inserted STOP-tetO cassette contained the following sequences in order: *loxP*, *FRT*, a neomycin resistant gene, *STOP*, *FRT*, *tetO*, and *loxP*. This targeting vector was introduced via electroporation into the ES cell line derived from C57BL/6 (RENKA) and the transduced cells were selected by G418.[21),22] PLD4-knock-in ES cells were identified by Southern blot analysis (Supplemental Fig. 1B). The selected ES cell line was injected into eight-cell stage embryos of ICR mouse strain, and chimeric mice of 100% ES cells were crossed with ICR mice to confirm germline transmission. Mice with germline transmission were backcrossed with C57BL/6N mice. Genotypes of the generated PLD4 knock-in homozygous (PLD4-deficient) mice were determined by Southern blot analysis. The PLD4-deficient mice were born in predicted Mendelian ratios. As shown in Fig. 1B and 1C, qRT-PCR

using specific primer sets and Western blot analyses demonstrated that PLD4 expression was completely suppressed at the mRNA as well as protein level in the adult homozygous animals. Expression patterns of PLD1, PLD2, and PLD3 were examined by qRT-PCR (Fig. 1D–F). The mRNA expression level of these PLD members were unchanged in the adult brains of PLD4-deficient mice, although a significant increase in the liver and decrease in the thymus was observed for PLD1 and PLD3, respectively.

The PLD4-deficient mice were born healthy, and had no apparent signs or symptoms during development through adulthood. In the initial several generations, the heterozygote or homozygote males often showed significant weight gain with splenomegaly after 4 weeks of age, but these phenotypes disappeared after multiple generations had passed (data not shown).

Change in microglial activation in PLD4-deficient mice. At P7, when PLD4 mRNA is typically upregulated in the cerebellum,[2),6)] no significant differences in gross brain structure were observed in PLD4-deficient mice compared to wild type (Fig. 2A, B). In the cerebellum, normal formation of the cortical layers including the molecular, external and internal granule layers was observed in PLD4-deficient mice (Fig. 2B, right).

Microglial activation in cerebellum was examined by immunostaining with an anti-Iba1 antibody at P5 and P7. At P5, activated rounded microglia were spread diffusely throughout the cerebellar white matter in both wild type and PLD4-deficient mice (Fig. 2C–F, K). At P7, rounded microglia that were strongly Iba1-positive could still be observed in the white matter that surrounds the deep cerebellar nuclei (deep white matter) of PLD4-deficient mice, whereas Iba1 staining intensity was reduced in most of the wild type microglia in the same area (Fig. 2G–J, L). At P10, process-bearing ramified microglia were found in both types of mice (Supplemental Fig. 2).

Microglial activation induces two phenotypes: M1 microglia and M2 microglia.[26)–29)] M1 microglia show an inflammatory phenotype and secrete proinflammatory cytokines, including iNOS, TNFα, IL-1β, IFNγ and surface markers CD16, CD32, CD68, and CD86. In contrast, M2 microglia have an anti-inflammatory phenotype, and express different molecules such as IL-4, arginase 1, Ym1, CD163, CD206, and IL10.[27),30)–32)] In order to determine the type of activated microglia present in the PLD4-deficient or wild type mice, sections were double-immunostained with an anti-Iba1 antibody and the microglial marker antibodies anti-CD68 or anti-arginase 1. Staining intensity of each CD68-positive cell was measured as described in Materials and methods. All Iba1-positive cells (red) were also positive for CD68 (green) in the deep white matter (Fig. 3A, B) and cerebellar folia (Fig. 3D, E) of both genotypes at P5. However, the signal intensity of CD68 was significantly lower in the Iba1-positive cells of PLD4-deficient mice than in wild types at P5 (Fig. 3C, F). Thus, wild type microglia showed high expression of CD68 while most of the PLD4-deficient microglia contained only low levels of CD68. No Iba1-positive microglia showed arginase 1 immunoreactivity in either genotype at P5 (data not shown).

These results suggest that while microglia were activated during postnatal development, the pattern of activation was affected by PLD4-deficiency. Given that arginase 1 reactivity was not observed in Iba1-positive cells of either genotype, this suggests that activated microglia temporarily appeared during development but did not show the typical arginase 1-positive M2 phenotype.

Neurons and astrocytes in the PLD4-deficient cerebellum. During development, microglia are actively involved in apoptosis of excessive neurons and axonal pruning during the final stages of neuronal circuit formation.[8)] Since inhibition of PLD4 by siRNA treatment caused partial reduction of phagocytic activity in microglia *in vitro*,[6)] we examined the development of Purkinje cells in PLD4-deficient mice. At P5 and P7, Calbindin immunostaining showed formation of the Purkinje cell layer with extension of the dendrites and axons (Fig. 4A–D, see also A'–D' for higher magnification views of the Purkinje cell layer). No obvious changes were observed in the two groups. In addition, the thickness of both the external and internal granule cell layers, as visualized by DAPI staining, were also unchanged (see DAPI staining of P7 cerebella in Fig. 2G–J). Calbindin-positive dendrites and axons were developed similarly at P10 (Supplemental Fig. 2E, F).

Astrocytes and Bergmann glia were examined by immunostaining with an anti-GFAP antibody. The GFAP staining pattern and intensity was similar between PLD4-deficient and wild type mice (Fig. 4E–J, Supplemental Fig. 2G–J).

These results demonstrate that while the loss of PLD4 alters the phenotype of activated microglia, astrocytes and neurons do not appear to be affected.
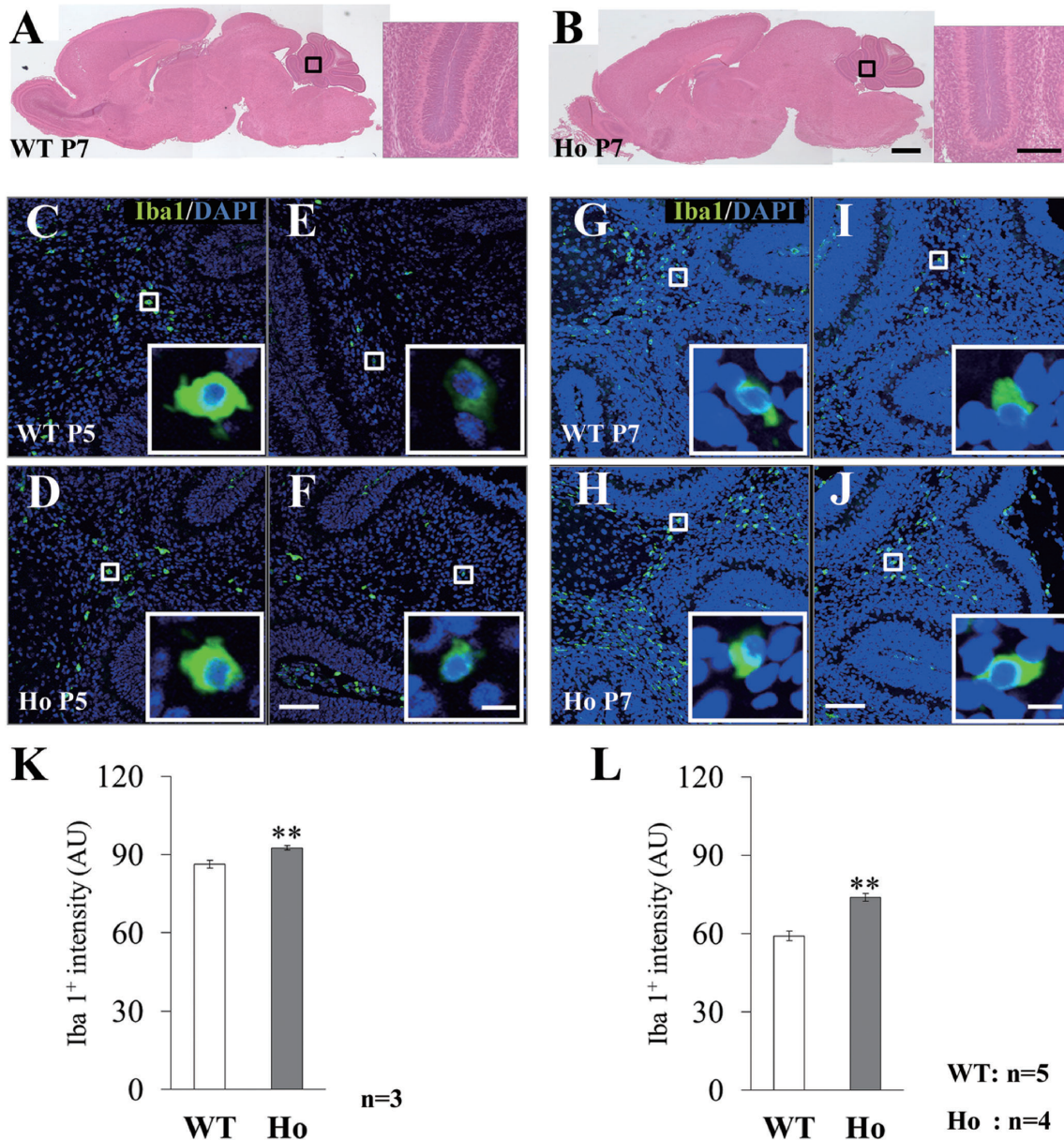
Fig. 2. Microglial activation in the cerebella of PLD4-deficient mice. **(A, B)** Comparison of gross brain structures in wild type (WT; A) and PLD4-deficient mice (Ho; B) at P7. Paraffin sections were stained with hematoxylin and eosin. High magnification images of cerebellar cortex (black squares) are shown in the right panels. No significant differences in gross brain anatomy were observed. Scale bars in B and in the higher magnification images at right represent 500 µm and 100 µm, respectively. **(C–J)** Iba1-positive microglia in P5 (C–F) and P7 (G–J) cerebella. Frozen sections of deep white matter (C, D, G, H) or folial white matter (E, F, I, J) of the cerebella obtained from wild type (C, E, G, I) and PLD4-deficient (D, F, H, J) mice were immunostained using an anti-Iba1 antibody. A representative Iba1-positive cell indicated by the white square in each panel is shown at higher magnification in the right lower corners. Note that microglia at P5 and P7 are the rounded activated type. Scale bars represent 100 µm (F, J) or 10 µm (in the white squares of F, J). **(K, L)** Intensity of Iba1 immunoreactivity in individual cells of the deep cerebellar white matter at P5 (K) and P7 (L). Graphs indicate the mean ± SEM. Data were obtained from: 92 WT cells and 98 Ho cells at P5, and 125 WT cells and 130 Ho cells in L (n = indicates number of mice examined). Statistical analysis was performed using a student t test. **P < 0.01.
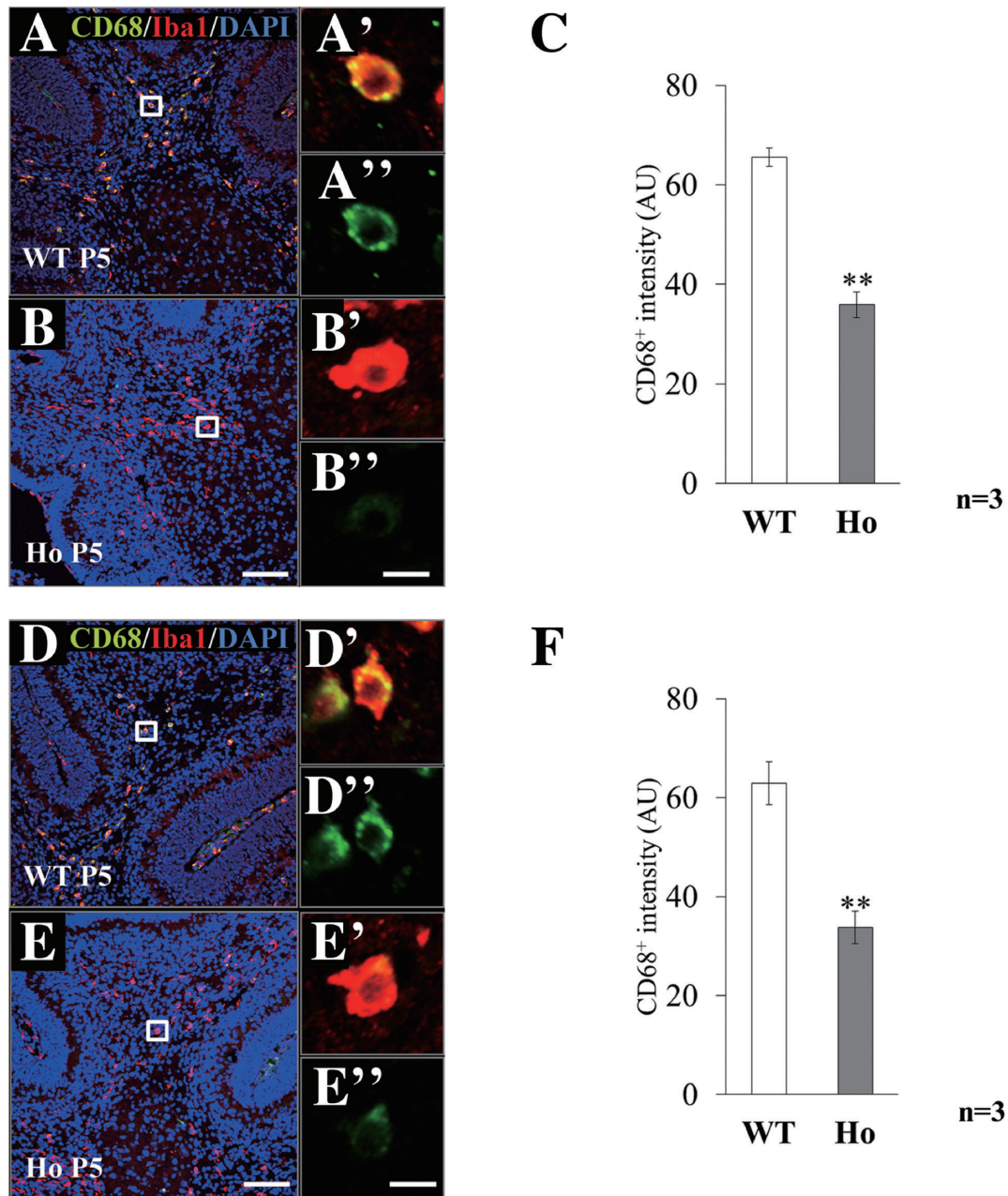
Fig. 3. CD68 immunoreactivity of the cerebellar microglia in PLD4-deficient mice. **(A–F)** Double-labeling of cells by anti-Iba1 (red) and anti-CD68 (green) antibodies in the deep white matter (A–C) and folial white matter (D–F) of P5 cerebellum obtained from wild type (A, D) or PLD4-deficient (B, E) mice. (A'–E', A''–E'') Higher magnification images of representative Iba1+CD68+ cells from the white squares in A–E. Scale bars in B, E and B'', E'' are 100 μm and 10 μm, respectively. All Iba1-positive cells were also positive for CD68, however, the staining intensity of CD68 (see Materials and methods) in PLD4-deficient cells was significantly lower than in wild type cells (C, F). Thus, the phenotype of activated microglia in PLD4-deficient mice is different from that of wild type. Data were obtained from: 78 WT cells and 65 Ho cells in the deep white matter (C), and 25 WT cells and 32 Ho cells in the folia (F) (n = number of mice examined). Graphs indicate mean ± SEM. Statistical analysis was performed using a student *t* test. **P < 0.01.
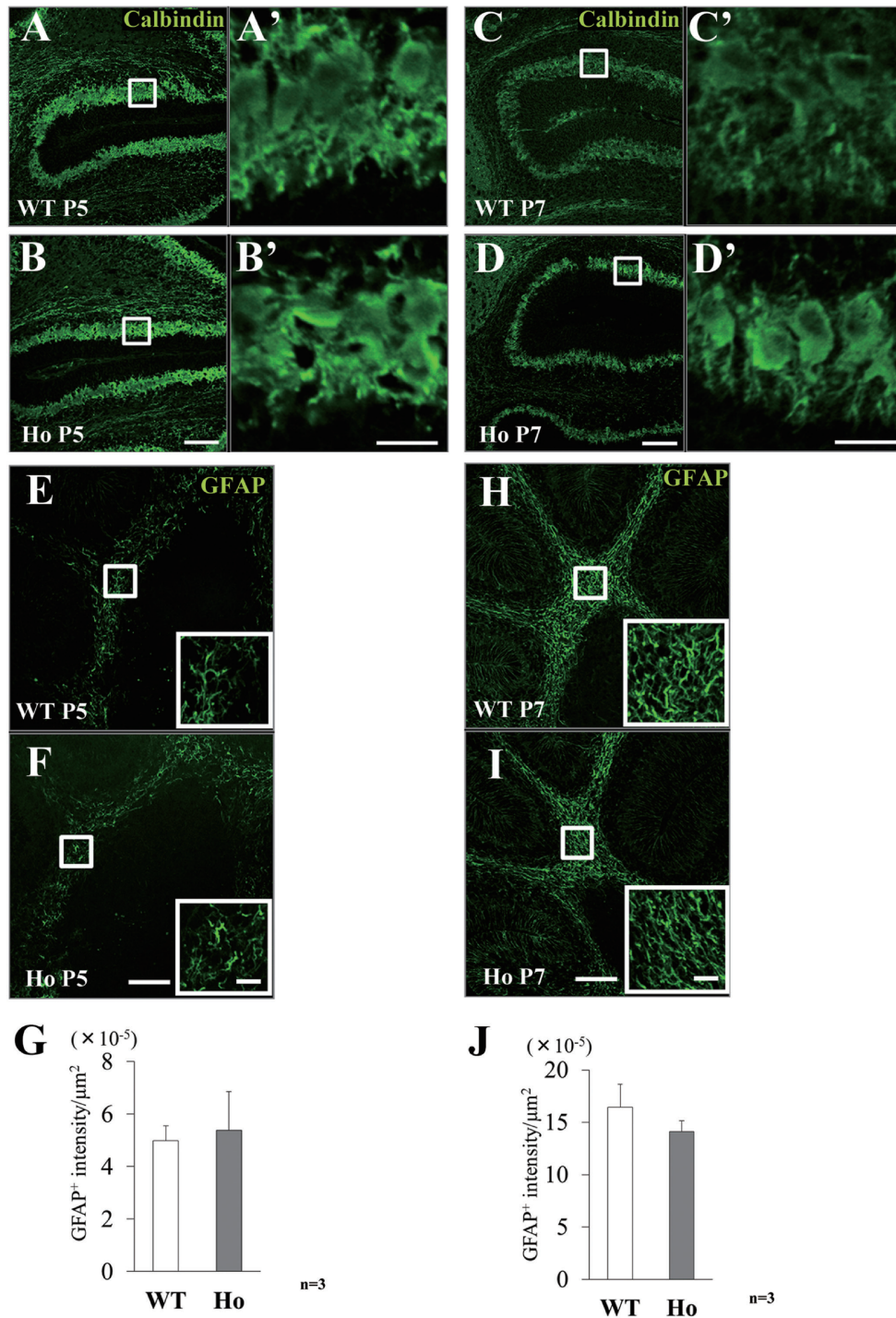
Fig. 4.   Purkinje cells and astrocytes in the cerebella of PLD4-deficient mice. **(A–D)** Representative calbindin-positive Purkinje cells in wild type (WT; A, C) and PLD4-deficient (Ho; B, D) cerebella at P5 (A, B) and P7 (C, D). A' to D' are higher magnification images of the white squares in A to D. No apparent differences were observed between wild type and PLD4-deficient mice at either age. Scale bars indicate 100 µm (B, D) or 20 µm (B', D'). **(E–J)** GFAP immunoreactivity in astrocytes from the deep white matter of wild type (E, H) and PLD4-deficient (F, I) cerebella at P5 (E, F, G) and P7 (H, I, J). Higher magnification images of the white squares are shown in the lower right corners. Intensity of GFAP immunoreactivity in the deep white matter was quantified and is represented as intensity per unit area (G, J). Graphs in G and J indicate the mean ± SEM. Statistical analyses with student t tests showed no significant difference between the two genotypes at either age.
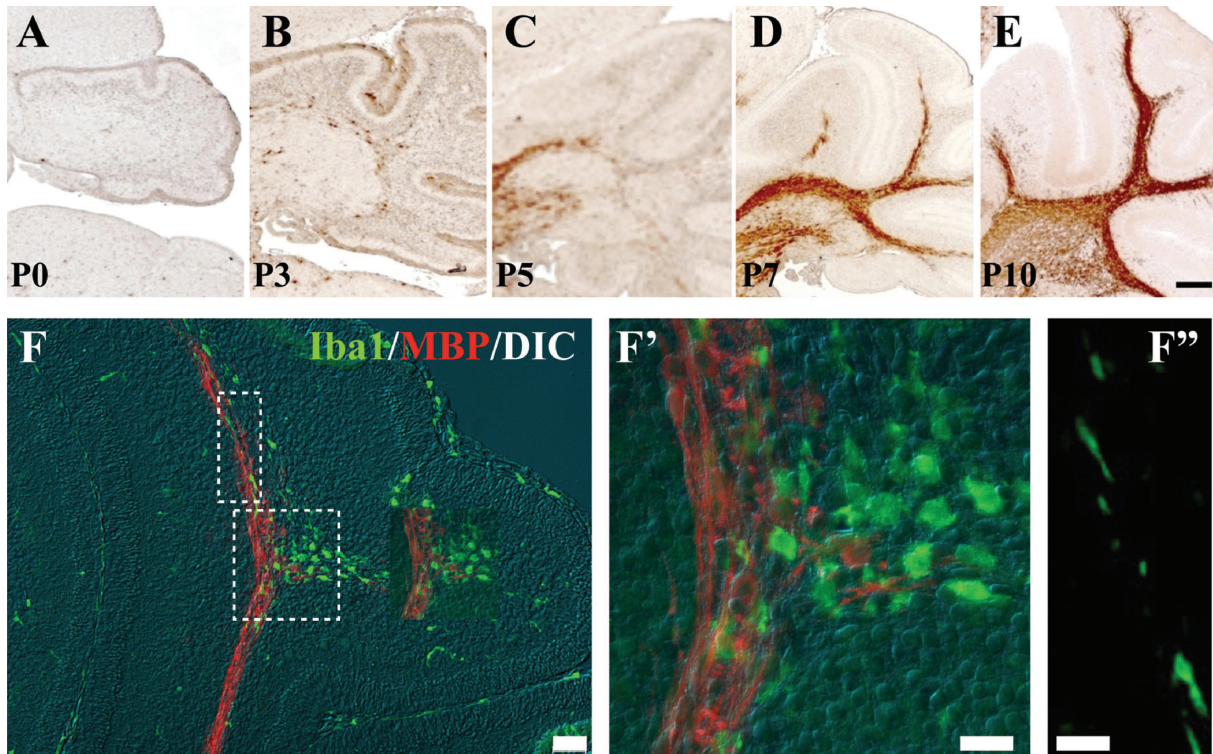
Fig. 5. Relationship between myelination and microglial activation during mouse cerebellar development. **(A–E)** Progress of myelination in normal C57BL mouse cerebellum. Frozen sections obtained from P0 (A), P3 (B), P5 (C), P7 (D) and P10 (E) were immunostained with an anti-MBP antibody. Scale bar in E represents 200 µm. **(F, F', F'')** Double immunostaining of the white matter in cerebellar folia at P7 with anti-Iba1 (green) and anti-MBP (red) antibodies. Images are also shown with DIC overlays (F and F'). F' and F'' (single Iba1 image) indicate higher magnification of the white dotted squares in F. Note that myelination in the folial white matter is in progress and clusters of rounded activated microglia are mainly found at the myelination fronts (F') but not in already myelinated area (F''). Scale bars indicate 50 µm (F) and 20 µm (F', F'').

Correlation of microglial activation and myelination in the cerebellum. It is well known that activated microglia transiently appear during cerebellar development, and in our previous study, we showed that PLD4 expression is upregulated in these cells. In that study, a small number of PLD4 mRNA-positive cells first appeared in the proximal region of the white matter at P3, and became widely distributed within the folia from the deep white matter to the distal white matter at P5 and P7. By P10, they had dispersed into the gray matter.[6] Since cerebellar myelination also occurs during the early postnatal period, we examined the myelination process by immunostaining with an anti-MBP antibody in C57BL/6 mice at various ages from P1 to P10 (Fig. 5A–E). MBP-positive oligodendrocytes appeared at P3 from the boundary of the brainstem. At P5, myelination occurred in the deep white matter around the cerebellar nucleus, then progressed into

the white matter of the folia and spread to the tips by P7. Myelination ultimately reached the axons perforating into the internal granule cell layers at P10. These temporal changes were consistent with the presence of rounded Iba1-positive or PLD4-positive activated microglia (Fig. 2).[6] Interestingly, double immunostaining with anti-Iba1 and anti-MBP antibodies clearly showed that a mass of activated microglia was often present at the myelination front in folia at P7 (Fig. 5F, F'), while slender-shaped microglia were present in the already myelinated areas (Fig. 5F'').

Thus, the timing of microglial activation and myelination shows a significant correlation during development, especially at the myelination front. Moreover, the shapes of the microglia appear to be influenced by the presence or absence of myelin.

Influence of PLD4-deficient microglia on myelination. Since the activation of microglia is

well correlated to the timing of myelination, especially at the myelination front, we examined the influence of PLD4-deficient microglia on myelination. Western blot analysis using an anti-MBP antibody showed no significant difference in P7 cerebella of wild-type and PLD4-deficient mice (Fig. 6A, B). In contrast, immunostaining with an anti-MBP antibody did show a difference between wild type and PLD4-deficient cerebella during the myelination process. In wild types, MBP-positive myelin membranes were found in the deep white matter at P5 (Fig. 6C, C'), whereas in PLD4-deficient mice, MBP-positive cell bodies of premyelinating oligodendrocytes were common and less myelin membrane staining was observed (Fig. 6D, D', white arrowheads). At this stage of development, individual difference was observed in mice of both genotypes, however, 4 out of 5 mice from each group showed the same result as depicted in the figure, suggesting that these differences were significant. At P7, myelin membranes were found in the deep white matter around the cerebellar nuclei of both genotypes (Fig. 6G, H, green) and in the white matter of the folia in wild types (Fig. 6E, E'), whereas MBP-positive premyelinating oligodendrocyte cell bodies were frequently found in the folia of PLD4-deficient mice (Fig. 6F, F', white arrowheads). Double immunostaining of P7 cerebella using anti-MBP and anti-Iba1 antibodies showed that in both types of mice rounded activated microglia were found adjacent to the myelinated areas in the folia and near the internal granule layers where myelination would occur in the near future (Fig. 6G, G', H, H'). These results suggest a delay in the onset of myelination in PLD4-deficient mice compared with the timing in wild type mice.

Similar results were obtained in the PLD4-deficient corpus callosum at P7 (Fig. 7). MBP-positive myelin was found in wild type mice whereas MBP signals were still restricted in their cell bodies and less myelin was observed in the PLD4-deficient mice (Fig. 7A, B). For quantitative analysis, numbers of premyelinating oligodendrocytes with MBP-positive cell bodies were counted in the corpus callosum at three different positions in each brain (Fig. 7C). In all the positions, significant numbers of MBP-positive cells remain premyelinating oligodendrocytes in the PLD-deficient mice (Fig. 7D). Thus, the delay of myelination in the corpus callosum was more prominent than in the cerebellum, likely attributed to the later onset of myelination in corpus callosum.

Discussion

This study used PLD4-deficient mice to show a mild but significant delay in the onset of myelination in the cerebellum and corpus callosum. PLD4-deficient microglia are still activated in the developing brain, however, the activation pattern is altered. Thus, the present study suggests that activated microglia in the developing white matter may have a role in the initial stages of myelination, especially at the myelinating front, possibly via a PLD4-related mechanism.

In the developing cerebellum, Iba1-positive activated microglia from wild type and PLD4-deficient mice showed different characteristics based on CD68 expression levels. CD68 is a 110 kDa glycoprotein present on the lysosomal membrane and cell surface of myeloid cells including tissue macrophages, monocytes, and neutrophils.[33]–[35] It is also commonly used as a marker for activated microglia.[36],[37] Because PLD4 is present in cytoplasmic vesicles along with early endosomal markers, as well as in phagosomes, it will be important to elucidate the relationship between these molecules.

Transient microglial activation is a well-known phenomenon in the developing brain.[7]–[10],[38] Many studies have been conducted to look at the role of these transiently activated microglia during development, but these studies mainly focused on their involvement in neuronal events, including neurogenesis, neuronal death, neurite growth, and synaptic or axonal pruning.[8],[9] Our present study shows that activated microglia in the P7 cerebellum are often found at the myelination front, and microglia are transformed into a slender morphology in regions where MBP-positive myelin sheaths are present (Fig. 5). At the myelination front, activated microglia and oligodendrocytes with MBP-positive cell bodies (premyelinating oligodendrocytes) are found in close proximity. Thus, during early stages in the postnatal cerebellum, activated microglia are mainly present in the white matter near axons that will soon be myelinated. Although further studies using various differentiation-specific oligodendrocyte markers are needed to show how and in which stage myelination is affected in these mice, the delayed myelination observed in PLD4-deficient mice indicates a correlation between activated microglia and onset of myelination. This change is significant, and found also in corpus callosum, but only persists for several days during early neonatal development in this mutant line. Myelination is
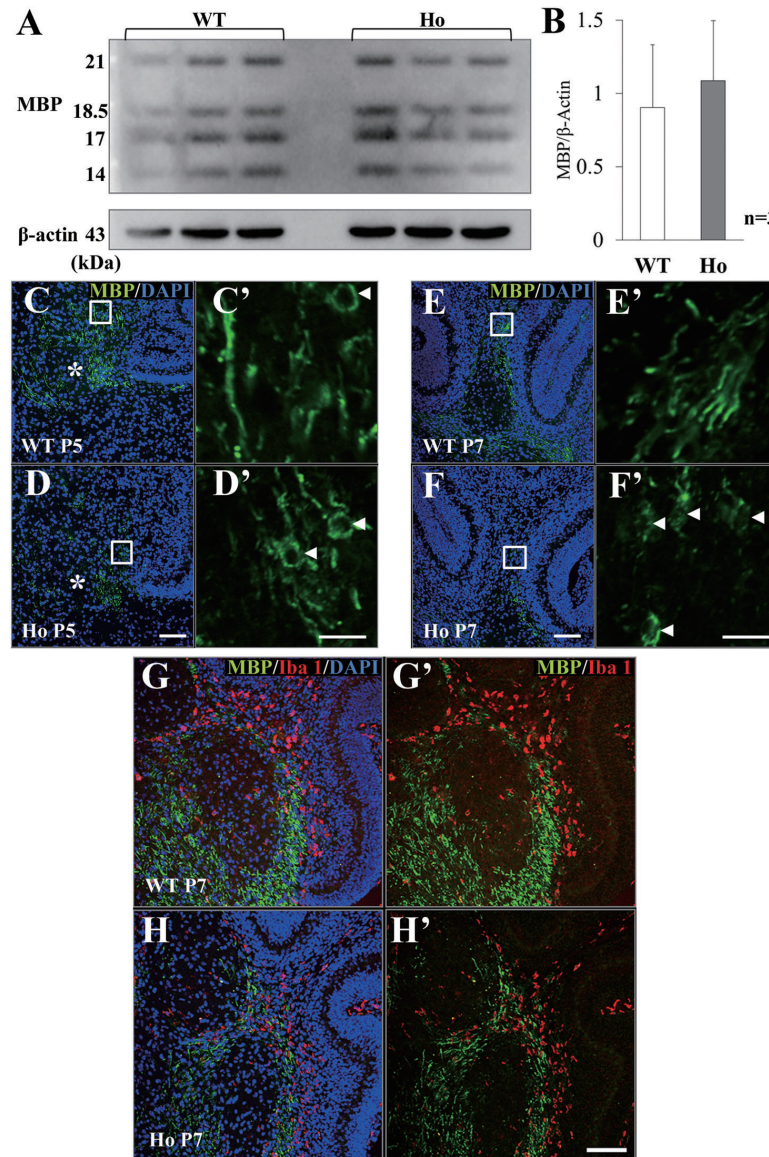
Fig. 6.   Influence of PLD4 deficiency on cerebellar myelination. **(A, B)** Western blot for MBP in the cerebellum of P7 wild type (WT) and PLD4-deficient (Ho) mice. Cerebellar homogenates (10 μg) from individual mice (three mice from each group) were separated by 12% SDS-PAGE and Western blot was performed using an anti-MBP antibody. After stripping off the antibody, the same blot was restained with an anti-β-actin antibody for quantification. B. The total intensity of all MBP bands (14, 17, 18.5, and 21 kDa) was quantified for each animal and the ratio of MBP to β-actin for each genotype was calculated. Graph indicates mean ± SEM. Statistical analysis with a student *t* test shows no significant difference between the two groups. **(C–F)** Comparison of MBP immunoreactivity in wild type (C, E) and PLD4-deficient (D, F) cerebella at P5 (C, D) and P7 (E, F). Cell nuclei are stained with DAPI (blue). Representative images of 5 mice from each genotype were selected. As shown in Fig. 5C and D, myelination in the deep white matter is in progress at P5 and progresses to the folial white matter by P7. Images in C, D or E, F show the deep white matter tracts, or folial white matter, respectively. C'–F' are higher magnification views of the white squares in C–F without DAPI. At P5, MBP-positive myelin membranes were found in the deep white matter in wild type mice, while premyelinating oligodendrocytes with MBP-positive cell bodies (white arrowheads) were present in PLD4-deficient mice. At P7, myelin membranes were present in wild type folia, whereas premyelinating oligodendrocytes (white arrowheads) were still found in PLD4-deficeint mice in the same region. * represents the border between the cerebellum (upper) and the earlier myelinating brainstem (lower). Scale bars indicate 100 μm (D, F) and 20 μm (D', F'). **(G, H)** Double immunostaining of P7 wild type (G) and PLD4-deficient (H) cerebellar deep white matter around the cerebellar nuclei using anti-MBP (green) and anti-Iba1 (red) antibodies. The DAPI staining pattern is overlaid to indicate the cerebellar region. G' and H' are the same images as in G and H without DAPI. In mice of both genotypes, clusters of rounded Iba1-positive activated microglia are present in the area where myelination is progressing. Scale bar in H' represents 100 μm.
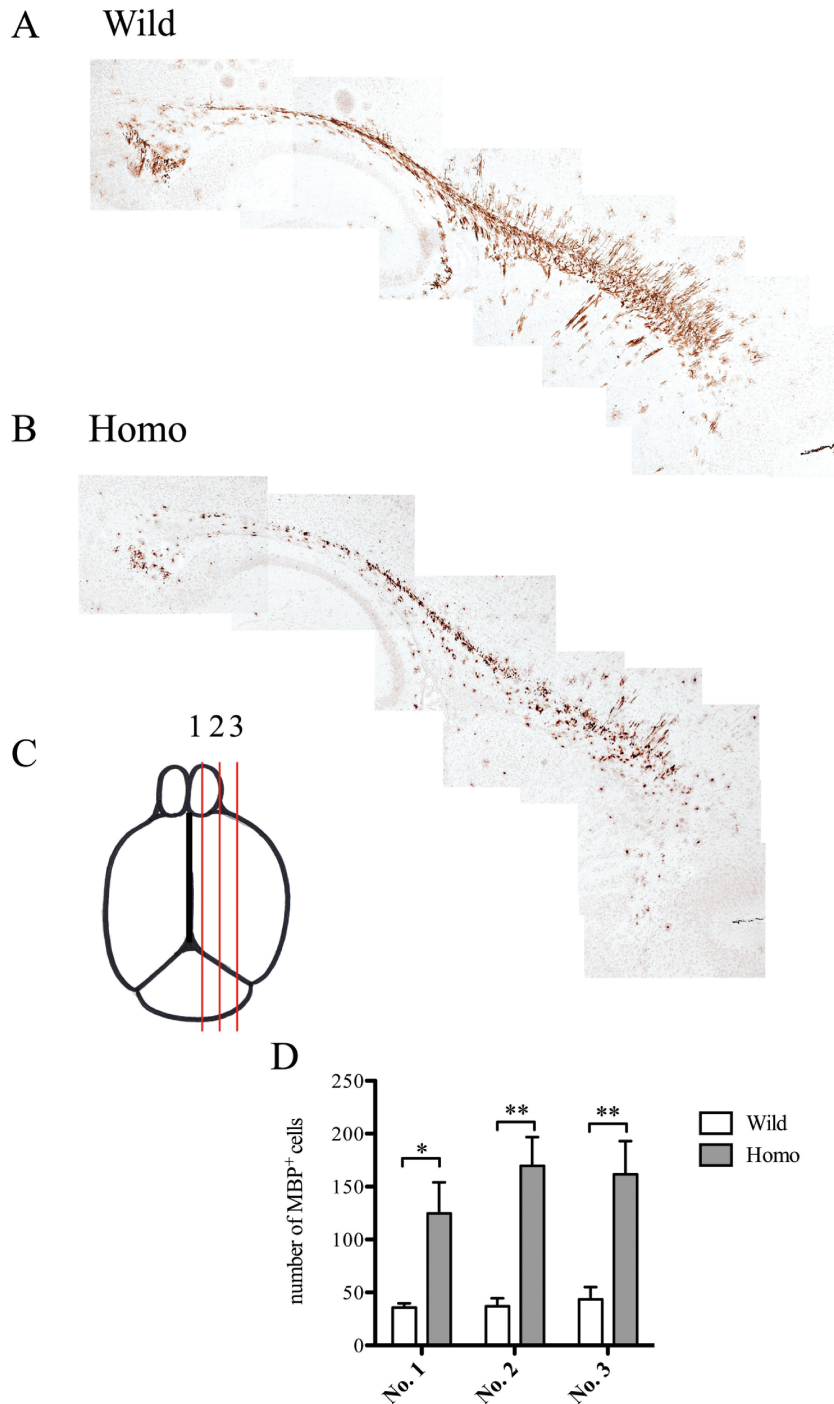
Fig. 7.   Delayed myelination in the corpus callosum of P7 PLD4-deificent mice. **(A, B)** Sagittal sections of paraffin-embedded brains obtained from wild type (WT; A) and PLD4-deficient (Ho; B) mice were immunostained with an anti-MBP antibody. Brain sections from 4 mice of each type were examined, and representative images of the MBP-stained corpus callosum (forefront at right side) are shown. **(C)** Sagittal sections from three different regions (1 to 3) of each sample were identified based on the histological shape of the cerebellum. Sections from position No. 1 were characterized by having a cerebellum with 5 folia, position No. 2 had 6 folia, and position No. 3 had 7 folia. **(D)** MBP signals were restricted to the cell bodies of premyelinating oligodendrocytes, and these signals were diminished in myelinating oligodendrocytes. The numbers of premyelinating oligodendrocytes with MBP-positive cell bodies were counted in the corpus callosum at the three positions. Graphs indicate mean ± SEM. Two-way ANOVA with Bonferroni multiple comparison tests were used for statistical analyses. *P < 0.05, **P < 0.01.

strictly regulated by local cues from axons or other glial cells.[17]–[19] In pathological conditions, microglia/macrophages can also promote remyelination.[28],[29],[39] Although it is not clear how PLD4-deficient microglia affect the onset of myelination, phagocytosis of microglia may be important since down-regulation of PLD4 expression by siRNA treatment partially inhibited phagocytosis *in vitro*.[6] In addition to cleaning up the pruned axonal branches or apoptotic cells prior to myelination, it is possible that activated microglia may also provide localized cues for oligodendrocytes to begin myelin formation either by direct contact or by secretion of humoral factors. Our data suggest that PLD4 may be involved in this series of events. Once this critical step is completed, oligodendrocytes may continue to myelinate without disturbance and could eventually catch up around P10 in PLD4-deficient mice (data not shown). Moreover, once myelin is formed, microglia are no longer activated, and switch to a resting state.

Under pathological conditions, microglia act as a double-edged sword as they release either pro-inflammatory or anti-inflammatory factors which can accelerate or protect against brain damage.[29] These two types are referred to as M1 and M2 microglia, respectively. In demyelinating conditions, a predominance of the M2 type of microglia improves clinical outcomes and oligodendrocyte differentiation.[28],[40],[41] However, the phenotype of microglia within the developing brain is still unknown. Arginase 1 is one of the markers for M2 microglia. Activated microglia found in the P5 mouse cerebellum showed no arginase 1 immunoreactivity in either wild type or PLD4-deficient mice, suggesting developing microglia are not of the typical arginase 1-positive M2 phenotype. An *in vivo* study by Shigemoto-Mogami *et al.*[10] suggested potential candidates, including proinflammatory cytokines IL-1β, IL-6, TNFα, and IFNγ in the promotion of oligodendrogenesis as well as neurogenesis in the early postnatal subventricular zone. In contrast, a study using freshly isolated microglia showed that P3 microglia expressed relatively high iNOS, TNFα and arginase 1, indicating that developmental microglia did not exclusively express M1 or M2 phenotypic markers.[26] Thus, further study is needed to confirm the phenotype of activated microglia during development. Identifying the factors involved in delaying myelination in PLD4-deficient mice will be the next step in elucidating its function. In addition, PLD4 was shown to be upregulated in activated microglia

under demyelinating conditions caused by PLP overexpression.[6],[42] Studies into the role of PLD4 during the demyelination-remyelination process are presently under way.

Supporting information

Probe sequences for Southern blot analysis.
5′-probe (722 b):
TTAGTGTAATGAGCTGAATAAACCCCTAGC-
ATACCCATGGTCTATTCTTTTTGCTTAAAA-
AAAAAATGTAAGTATTAATCCAAGCACTTC-
CCCAGGTGCTGGTCACAGAGAAACCCAGT-
GTTGCTGTTGGGATCCGAGCCCTGTGGGTC-
CTGTGGTTCTCATGGTTCTGTGGTTCTTGT-
CCCCCTCTCCTGCAGTCATATGGCGTAGAG-
CTCATAAACCTTCCTTATCCAGCACACCAG-
GGCAGCCAGGGCTACTGTCTGTGCAGTCT-
CTTTCTGTACAGGTCGTCCTCCCGAACCGG-
CAGCGCTGGTGTGGAGGAGGTGAGCGCGT-
GCAGAGGCCGACTGGACAGTTTGTACGCAT-
CATACTACAGCTGGTACTTGTAGCCAGGGC-
CAAACTGCCAGGAGATCCTATAGAGGGTCC-
AGCAGTGGACAGGGAGATGTAGTGGAAGT-
GGTCCAGGGGCAGTACCAATGGGGTGAAG-
AGGCAGGCAGTACCCGATAACACGGCCATC-
TTGTGCAGGCAATTGTCTATGGTGATCCAG-
AGGGCTGTCTCATCTCCAGTTCGGGTGGGC-
TCTATCACAATGTACTTACACTGGGCTTCC-
AGCGCCTGCTCCAGCTCACACTCACACTGG-
TCCCGGGCGTTCTCCCCACTGCAGATTTCA-
TGCACTATGTAGCAGCCTGCAGCTGGGAGC-
TGTGGCCACCCAGACCCAGAAGCCTCCTTC-
CCTAC
3′ probe (622 b):
ATCATTAAGGTTATGACCTTGACTGTCTAG-
AGAGAGGGGTCTCAGGGAAGCCTGTATCTT-
TGTTTTCTCACCTGCAACAGCCTTGATCAG-
TGGGGTCATTCTGAGGGTAAAATGAATGAA-
CACCAACAGGGGCAGAGGGACCGGGGCAG-
ATCTATTAGGCAGTTCTGAAGTTAGCATTA-
AAGAGCTGGCTCTCCATCTGTCCATCCATC-
CATTTATCTATTTGTCTCCTGCAGGTGCCC-
AGATACGACAAGTGCCCATGAAACAGCTTA-
CTGGGGGTGTTCTACACTCCAAATTCTGGG-
TTGTGGATGGGCGACACATCTACGTGGGCA-
GTGCCAACATGGACTGGCGGTCCCTGACTC-
AGGTGGGTCCCAAGGCCCAGGGATAGGATG-
AGGCCCAGGGGCAGCTTCTCCCCTCGCCAT-
CTCCAAGGGCTGCTGTTTCTGAAGAAAGCT-
GGTACTGGGAGGAGTTAGCAAGCAGAACCT-
TGGGTCACACACCGTTTTTGCCATACCACC-
ATAGCAGGGCCAATCAGAGTTGGTCCCACC-
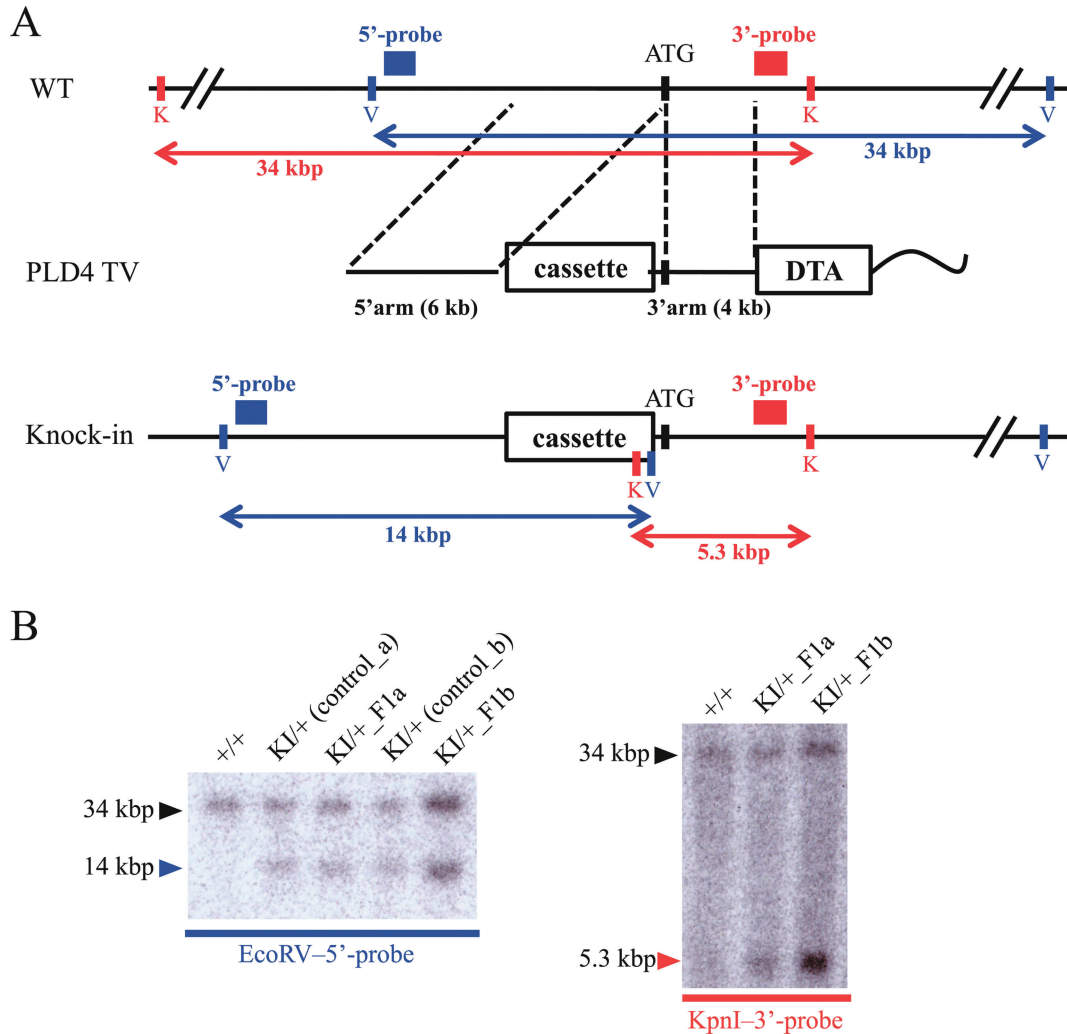
Supplemental Fig. 1. Generation of PLD4-targeted knock-in mouse. **A.** Schematic diagram of PLD4-targeting. PLD4-targeting vector (PLD4 TV) included diphtheria toxin A subunit (DTA) was produced using Flexible Accelerated STOP Tetracycline Operator (tetO)-knock in (FAST) system (see Materials and methods). After homologous recombination in ES cells, the STOP-tetO cassette (3.5 kbp) was inserted into just upstream of ATG in PLD4 locus by PLD4 TV. The restriction sites, the restriction products (two-headed arrows), and the positions of probes (boxes) for Southern blot analysis were indicated. V, EcoRV site; K, KpnI site. Each color corresponds to the color in B. **B.** Genotyping of obtained two PLD4 knock in mouse lines by Southern blot analysis. In first screening of targeted ES cells by PLD4 TV, eight positive clones were selected from G418-resistant 116 colonies. After second screening, two clones were selected to produce chimera mice. Genomic DNAs from obtained two knock-in mice (KI/+_F1a and KI/+_F1b) were analyzed by Southern blotting. The restriction fragments indicating insertion mutation [14 kbp (EcoRV–5'-probe, blue arrowhead) and 5.3 kbp (KpnI–3'-probe, red arrowhead) fragments] (see panel A) were detected in both lines. EcoRV-digested DNA fragments derived from two KI/+ ES cell colonies were used as control (a and b).

AGTTAGAAGGTTCTACATGACCCTGCACTC-
AGGCCCTGGGACAGCATGTTCAGGCCATGG-
CTCACAGGAAAACCACAGCTCAC
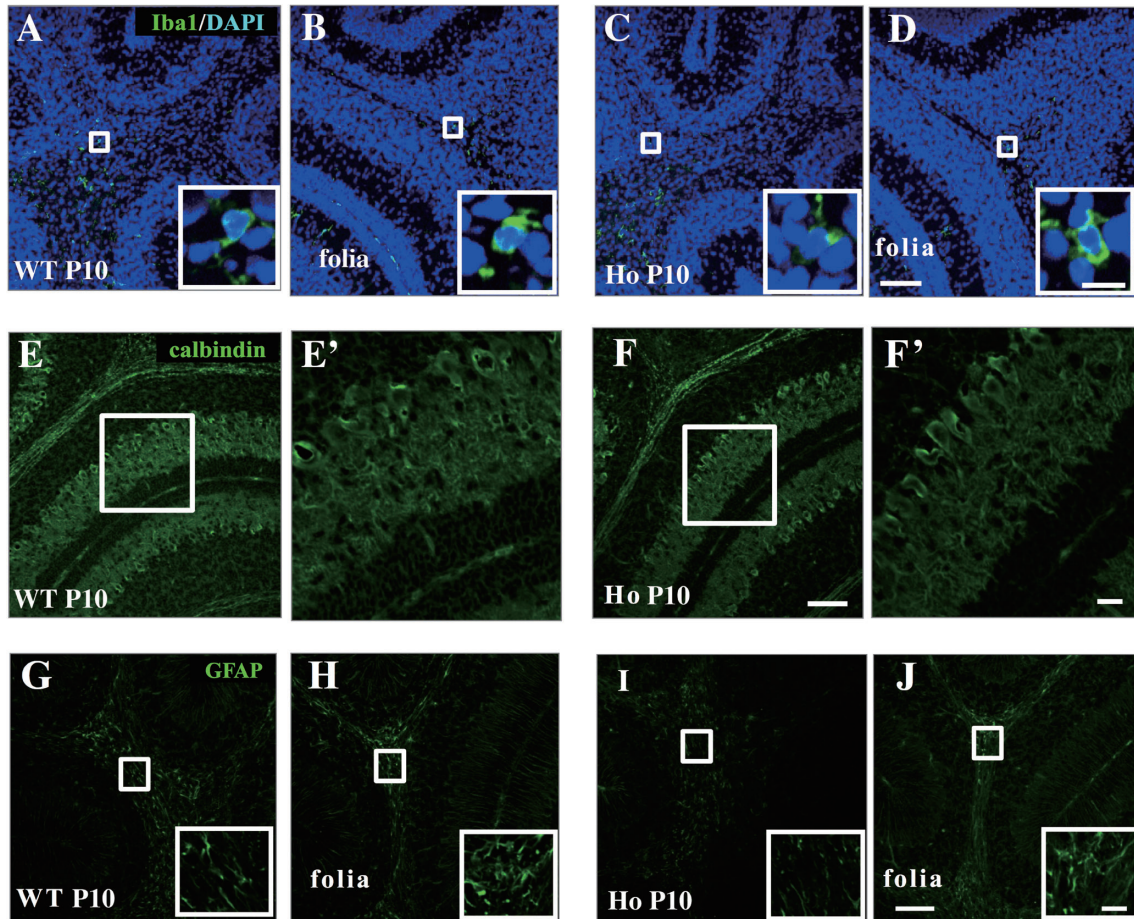
Supplemental Fig. 2. Characteristics of microglia, Purkinje cells, and astrocytes in the cerebella of PLD4-deficient mice at P10. Representative images of Iba1-positive microglia in wild type (WT; **A**, **B**) and PLD4-deficient (Ho; **C**, **D**) cerebella at P10 were exhibited. Higher magnification of a representative Iba1-positive microglia is shown in the lower right corner. At P10 process-bearing ramified microglia were found in both types of mice. Purkinje cells in WT (**E**) and Ho (**F**) cerebella at P10 were immunostained by anti-calbindin antibody (E, F). E' and F' are higher magnification images of the white squares in E and F. GFAP immunoreactive astrocytes in the deep white matter (**G**, **I**) and folial white matter (**H**, **J**) of WT and Ho mice were immunostained by anti-GFAP antibody. Higher-magnification images of white squares (G, H, I, J) were indicated in the lower right corners. No apparent differences of calbindin and GFAP positive staining were observed between two genotypes. Scale bars indicate 100 μm (D, F, J) or 10 μm (in the white squares of D) or 20 μm (F', in the white squares of J).

References

1) Sato, A., Sekine, Y., Saruta, C., Nishibe, H., Morita, N., Sato, Y., Sadakata, T., Shinoda, Y., Kojima, T. and Furuichi, T. (2008) Cerebellar development transcriptome database (CDT-DB): profiling of spatio-temporal gene expression during the postnatal development of mouse cerebellum. Neural Netw. **21**, 1056–1069.

2) Yoshikawa, F., Banno, Y., Otani, Y., Yamaguchi, Y., Nagakura-Takagi, Y., Morita, N., Sato, Y., Saruta, C., Nishibe, H., Sadakata, T., Shinoda, Y., Hayashi, K., Mishima, Y., Baba, H. and Furuichi, T. (2010) Phospholipase D family member 4, a transmembrane glycoprotein with no phospholi-

pase D activity, expression in spleen and early postnatal microglia. PLoS One **5**, e13932.

3) Frohman, M.A. (2015) The phospholipase D superfamily as therapeutic targets. Trends Pharmacol. Sci. **36**, 137–144.

4) Terao, C., Ohmura, K., Kawaguchi, Y., Nishimoto, T., Kawasaki, A., Takehara, K., Furukawa, H., Kochi, Y., Ota, Y., Ikari, K., Sato, S., Tohma, S., Yamada, R., Yamamoto, K., Kubo, M., Yamanaka, H., Kuwana, M., Tsuchiya, N., Matsuda, F. and Mimori, T. (2013) PLD4 as a novel susceptibility gene for systemic sclerosis in a Japanese population. Arthritis Rheum. **65**, 472–480.

5) Jung, S., Pausch, H., Langenmayer, M.C., Schwarzenbacher, H., Majzoub-Altweck, M.,

Gollnick, N.S. and Fries, R. (2014) A nonsense mutation in PLD4 is associated with a zinc deficiency-like syndrome in Fleckvieh cattle. BMC Genomics **15**, 623.

6) Otani, Y., Yamaguchi, Y., Sato, Y., Furuichi, T., Ikenaka, K., Kitani, H. and Baba, H. (2011) PLD4 is involved in phagocytosis of microglia: expression and localization changes of PLD4 are correlated with activation state of microglia. PLoS One **6**, e27544.

7) Perez-Pouchoulen, M., VanRyzin, J.W. and McCarthy, M.M. (2015) Morphological and phagocytic profile of microglia in the developing rat cerebellum (1,2,3). eNeuro **2**, 0036-00315.

8) Pont-Lezica, L., Béchade, C., Belarif-Cantaut, Y., Pascual, O. and Bessis, A. (2011) Physiological roles of microglia during development. J. Neurochem. **119**, 901–908.

9) Schafer, D.P., Lehrman, E.K. and Stevens, B. (2013) The "quad-partite" synapse: microglia-synapse interactions in the developing and mature CNS. Glia **61**, 24–36.

10) Shigemoto-Mogami, Y., Hoshikawa, K., Goldman, J.E., Sekino, Y. and Sato, K. (2014) Microglia enhance neurogenesis and oligodendrogenesis in the early postnatal subventricular zone. J. Neurosci. **34**, 2231–2243.

11) Kaur, C., Sivakumar, V., Zou, Z. and Ling, E.A. (2014) Microglia-derived proinflammatory cytokines tumor necrosis factor-alpha and interleukin-1beta induce Purkinje neuronal apoptosis via their receptors in hypoxic neonatal rat brain. Brain Struct. Funct. **219**, 151–170.

12) Lenz, K.M., Nugent, B.M., Haliyur, R. and McCarthy, M.M. (2013) Microglia are essential to masculinization of brain and behavior. J. Neurosci. **33**, 2761–2772.

13) Marín-Teva, J.L., Dusart, I., Colin, C., Gervais, A., van Rooijen, N. and Mallat, M. (2004) Microglia promote the death of developing Purkinje cells. Neuron **41**, 535–547.

14) Paolicelli, R.C., Bolasco, G., Pagani, F., Maggi, L., Scianni, M., Panzanelli, P., Giustetto, M., Ferreira, T.A., Guiducci, E., Dumas, L., Ragozzino, D. and Gross, C.T. (2011) Synaptic pruning by microglia is necessary for normal brain development. Science **333**, 1456–1458.

15) Schafer, D.P., Lehrman, E.K., Kautzman, A.G., Koyama, R., Mardinly, A.R., Yamasaki, R., Ransohoff, R.M., Greenberg, M.E., Barres, B.A. and Stevens, B. (2012) Microglia sculpt postnatal neural circuits in an activity and complement-dependent manner. Neuron **74**, 691–705.

16) Zhan, Y., Paolicelli, R.C., Sforazzini, F., Weinhard, L., Bolasco, G., Pagani, F., Vyssotski, A.L., Bifone, A., Gozzi, A., Ragozzino, D. and Gross, C.T. (2014) Deficient neuron-microglia signaling results in impaired functional brain connectivity and social behavior. Nat. Neurosci. **17**, 400–406.

17) Ahrendsen, J.T. and Macklin, W. (2013) Signaling mechanisms regulating myelination in the central nervous system. Neurosci. Bull. **29**, 199–215.

18) Nave, K.A. and Werner, H.B. (2014) Myelination of the nervous system: mechanisms and functions. Annu. Rev. Cell Dev. Biol. **30**, 503–533.

19) Taveggia, C., Feltri, M.L. and Wrabetz, L. (2010) Signals to promote myelin formation and repair. Nat. Rev. Neurol. **6**, 276–287.

20) Tanaka, K.F., Ahmari, S.E., Leonardo, E.D., Richardson-Jones, J.W., Budreck, E.C., Scheiffele, P., Sugio, S., Inamura, N., Ikenaka, K. and Hen, R. (2010) Flexible Accelerated STOP Tetracycline Operator-knockin (FAST): a versatile and efficient new gene modulating system. Biol. Psychiatry **67**, 770–773.

21) Mishina, M. and Sakimura, K. (2007) Conditional gene targeting on the pure C57BL/6 genetic background. Neurosci. Res. **58**, 105–112.

22) Kitayama, K., Abe, M., Kakizaki, T., Honma, D., Natsume, R., Fukaya, M., Watanabe, M., Miyazaki, J., Mishina, M. and Sakimura, K. (2001) Purkinje cell-specific and inducible gene recombination system generated from C57BL/6 mouse ES cells. Biochem. Biophys. Res. Commun. **281**, 1134–1140.

23) Yamaguchi, Y., Miyagi, Y. and Baba, H. (2008) Two-dimensional electrophoresis with cationic detergents, a powerful tool for the proteomic analysis of myelin proteins. Part 1: technical aspects of electrophoresis. J. Neurosci. Res. **86**, 755–765.

24) Yamaguchi, Y., Hayashi, A., Campagnoni, C.W., Kimura, A., Inuzuka, T. and Baba, H. (2012) L-MPZ, a novel isoform of myelin P0, is produced by stop codon readthrough. J. Biol. Chem. **287**, 17765–17776.

25) Ishibashi, T., Dupree, J.L., Ikenaka, K., Hirahara, Y., Honke, K., Peles, E., Suzuki, K., Nishino, H. and Baba, H. (2002) A myelin galactolipid, sulfatide, is essential for maintenance of ion channels on myelinated axon but not essential for initial cluster formation. J. Neurosci. **22**, 6507–6514.

26) Crain, J.M., Nikodemova, M. and Watters, J.J. (2013) Microglia express distinct M1 and M2 phenotypic markers in the postnatal and adult central nervous system in male and female mice. J. Neurosci. Res. **91**, 1143–1151.

27) Liao, B., Zhao, W., Beers, D.R., Henkel, J.S. and Appel, S.H. (2012) Transformation from a neuroprotective to a neurotoxic microglial phenotype in a mouse model of ALS. Exp. Neurol. **237**, 147–152.

28) Miron, V.E., Boyd, A., Zhao, J.W., Yuen, T.J., Ruckh, J.M., Shadrach, J.L., Wagers, A.J., Williams, A., Franklin, R.J. and ffrench-Constant, C. (2013) M2 microglia and macrophages drive oligodendrocyte differentiation during CNS remyelination. Nat. Neurosci. **16**, 1211–1218.

29) Miron, V.E. and Franklin, R.J. (2014) Macrophages and CNS remyelination. J. Neurochem. **130**, 165–171.

30) David, S. and Kroner, A. (2011) Repertoire of microglial and macrophage responses after spinal cord injury. Nat. Rev. Neurosci. **12**, 388–399.

31) Kigerl, K.A., Gensel, J.C., Ankeny, D.P., Alexander, J.K., Donnelly, D.J. and Popovich, P.G. (2009) Identification of two distinct macrophage subsets with divergent effects causing either neurotoxicity or regeneration in the injured mouse spinal cord. J. Neurosci. **29**, 13435–13444.

32) Ponomarev, E.D., Maresz, K., Tan, Y. and Dittel, B.N. (2007) CNS-derived interleukin-4 is essential for the regulation of autoimmune inflammation and induces a state of alternative activation in microglial cells. J. Neurosci. **27**, 10714–10721.

33) Holness, C.L. and Simmons, D.L. (1993) Molecular cloning of CD68, a human macrophage marker related to lysosomal glycoproteins. Blood **81**, 1607–1613.

34) Micklem, K., Rigney, E., Cordell, J., Simmons, D., Stross, P., Turley, H., Seed, B. and Mason, D. (1989) A human macrophage-associated antigen (CD68) detected by six different monoclonal antibodies. Br. J. Haematol. **73**, 6–11.

35) Matsumoto, H., Kumon, Y., Watanabe, H., Ohnishi, T., Shudou, M., Ii, C., Takahashi, H., Imai, Y. and Tanaka, J. (2007) Antibodies to CD11b, CD68, and lectin label neutrophils rather than microglia in traumatic and ischemic brain lesions. J. Neurosci. Res. **85**, 994–1009.

36) Graeber, M.B., Streit, W.J., Kiefer, R., Schoen, S.W. and Kreutzberg, G.W. (1990) New expression of myelomonocytic antigens by microglia and perivascular cells following lethal motor neuron injury. J. Neuroimmunol. **27**, 121–132.

37) Hoogland, I.C., Houbolt, C., van Westerloo, D.J., van Gool, W.A. and van de Beek, D. (2015) Systemic inflammation and microglial activation: systematic review of animal experiments. J. Neuroinflammation **12**, 114.

38) Ashwell, K. (1990) Microglia and cell death in the developing mouse cerebellum. Brain Res. Dev. Brain Res. **55**, 219–230.

39) Yuen, T.J., Johnson, K.R., Miron, V.E., Zhao, C., Quandt, J., Harrisingh, M.C., Swire, M., Williams, A., McFarland, H.F., Franklin, R.J. and ffrench-Constant, C. (2013) Identification of endothelin 2 as an inflammatory factor that promotes central nervous system remyelination. Brain **136**, 1035–1047.

40) Butovsky, O., Landa, G., Kunis, G., Ziv, Y., Avidan, H., Greenberg, N., Schwartz, A., Smirnov, I., Pollack, A., Jung, S. and Schwartz, M. (2006) Induction and blockage of oligodendrogenesis by differently activated microglia in an animal model of multiple sclerosis. J. Clin. Invest. **116**, 905–915.

41) Mikita, J., Dubourdieu-Cassagno, N., Deloire, M.S., Vekris, A., Biran, M., Raffard, G., Canron, M.H., Franconi, J.M., Boiziau, C. and Petry, K.G. (2011) Altered M1/M2 activation patterns of monocytes in severe relapsing experimental rat model of multiple sclerosis. Amelioration of clinical status by M2 activated monocyte administration. Mult. Scler. **17**, 2–15.

42) Kagawa, T., Ikenaka, K., Inoue, Y., Kuriyama, S., Tsujii, T., Nakao, J., Nakajima, K., Aruga, J., Okano, H. and Mikoshiba, K. (1994) Glial cell degeneration and hypomyelination caused by over-expression of myelin proteolipid protein gene. Neuron **13**, 427–442.